Experimental Mechanics
DOI 10.1007/s11340-014-9914-y

Direct Measurement of Opening Mode Stress Intensity Factors Using Flexoelectric Strain Gradient Sensors

Wenbin Huang · Shaorui Yang · Ningyi Zhang · Fuh-Gwo Yuan · Xiaoning Jiang

Received: 19 December 2013 / Accepted: 16 June 2014

Abstract This paper presents a new method for direct measurement of Mode-I stress intensify factor of cracks using $Ba_{0.64}Sr_{0.36}TiO_3$ flexoelectric strain gradient sensors. Firstly, strain gradient field around the opening mode crack tip was analyzed, followed by the derivation of induced flexoelectric polarization in the strain gradient sensors attached in the vicinity of a crack tip. It was found that the constant stress term makes no contribution to the strain gradient, thus the flexoelectric output directly reflects the singular effect. This unique property eliminates the special requirement for sensor placement coordinates and improves the accuracy of the stress intensify factor predication. A specimen with Mode-I crack was then prepared with two strain gradient sensors (4.7 mm×0.9 mm×0.3 mm) attached close to the crack tip to verify the analytical model for measurements of stress intensity factor. The experimental results matched well with the empirical estimation confirming that flexoelectric strain gradient sensing can be a convenient and accurate avenue for measuring the stress intensify factor.

Keywords Stress intensify factor · Crack sensing · Flexoelectric · Strain gradient sensing

Introduction

Cracks could cause a catastrophic failure of mechanical, civil, and aerospace structures. In reported inspections and major aircraft fatigue tests [1], 70 % of the damage discovered resulted from such cracks. As a parameter that indicates the amplification of the magnitude of the applied stress by special geometry, the stress intensity factors have often been used to predict the stress state near the tip of a crack caused by a remote load or residual stresses. They are useful for characterizing the strength of the structure and providing a failure criterion with the aim of not exceeding the fracture toughness of materials, which is a key parameter for designing fracture-safe structures. Numerical analysis including finite element method is usually used to obtain the stress intensity factors [2], with the known stress distribution in the vicinity of crack tip. However, it is difficult to obtain such stress/strain distribution information in a practical structure due to the complexity of structural configurations, applied loads and crack shapes. Several experimental techniques were then investigated to quantify the stress intensity factors by measuring stress/strain distributions, including photoelastic method [3], digital image correlation method [4], acousto-elastic method [5], thermoelastic method [6], strain gauge method [7] and piezoelectric method [8]. Among them, photoelastic method determines the stress intensity factors from their functional relationship with the displacement distribution from the optically measured isochromatic-fringe loop parameters at the crack tip. Digital image correlation method captures the real time two-dimensional crack opening displacement field and crack tip location during crack growth using camera, thus to deduce the corresponding stress intensity factors. However, the above two methods require optical equipment and high speed photographic recording system, which sometimes leads to a costly and bulky setup. On the other side, acousto-elastic method first calculates the shear stress field through measuring acoustic birefringence and angle, and then obtains the stress intensity factor from the series expansion of stress functions. It involves precise location of an acoustic transducer and needs a layer of viscous fluid for acoustic wave coupling between the transducer and the specimen. Therefore, these methods are more applicable to lab investigation instead of monitoring the stress intensity factors of in-service structures. Thermoelastic

W. Huang · S. Yang · N. Zhang · F.-G. Yuan (✉) · X. Jiang (✉)
Department of Mechanical and Aerospace Engineering, North Carolina State University, Raleigh, NC 27695, USA
e-mail: yuan@ncsu.edu
e-mail: xjiang5@ncsu.edu

Published online: 23 September 2014

method utilizes high precision infrared detectors to record the small temperature changes (tens of mK) near the crack tip induced by cyclic load, and further evaluates the stress intensify factors. It has an assumption of an adiabatic condition which is usually achieved by high frequency cyclic loading. In addition, thermal resolution, temperature of air and wind are usually concerns of thermoelastic method. In the piezoelectric method, stress or strain information is converted into electric signal of piezoelectric sensors. However, constant strain/stress term is not included in the analysis, which could mingle with singular components and hinder the accurate measurement of the stress intensity factors. In strain gauges methods, analysis procedures are developed for Mode-I cracks.

In this paper, flexoelectric strain gradient (SGS) sensors were developed for measurement of stress intensity factor of opening mode cracks. In principle, constant stress term makes no contribution to the strain gradient distribution, thus stress intensify factor can be obtained directly from measured polarizations of SGSs. Compared with strain gauge methods which need to be placed at certain special localizations in order to eliminate the effects of constant or higher order stress components, there is no such requirement for SGSs. Thus sensor mounting procedure may be simplified in a SGS method. In order to demonstrate this method, strain gradient field near the Mode-I crack tip and the corresponding SGS outputs were first analyzed. A specimen with Mode-I crack was then prepared with SGSs attached close to the crack tip to verify the analytical model for measurements of crack intensity factor.

Strain Gradient Sensing

In the stress localized area like a crack tip, a sharp stress change within a short distance would result in a very high strain gradient. Hence strain gradient can be a sensitive measurand for *in-situ* monitoring of initiation and progression of cracks. Flexoelectricity exactly offers a good avenue to directly measure the strain gradient, which should be favorable in structural health monitoring [9]. Similar to piezoelectricity, a well-known linear electromechanical interaction between electric polarization and mechanical stress or strain, flexoelectric effect refers to the linear relationship between electric polarization and mechanical strain gradient. Unlike piezoelectricity that is limit to 20 types of non-centrosymmetric point group, flexoelectricity exists in all solid materials and is represented as

$$P_l = \mu_{ijkl}\frac{\partial \varepsilon_{ij}}{\partial x_k} \tag{1}$$

where (ε_{ij}, $\partial\varepsilon_{ij}/\partial x_k$) are elastic strain and strain gradient, and μ_{ijkl} the flexoelectric coefficient. In 1964, Kogan first discussed the electric polarization induced in a centric crystal by inhomogeneous deformation [10]. Numerous studies have been performed since then on flexoelectric materials, structures, and devices [11–19].

For a centrosymmetric point group like *m3m*, the μ_{ijkl} tensor has only three independent components μ_{1111}, μ_{1122}, μ_{2323}, or in matrix notation μ_{11}, μ_{12}, μ_{44}. Thus, flexoelectric polarization can be written as follows:

$$P_i = \mu_{11}\frac{\partial \varepsilon_{ii}}{\partial x_i} + \mu_{12}\left(\frac{\partial \varepsilon_{jj}}{\partial x_i} + \frac{\partial \varepsilon_{kk}}{\partial x_i}\right) + \mu_{44}\left(\frac{\partial \varepsilon_{ji}}{\partial x_j} + \frac{\partial \varepsilon_{ki}}{\partial x_k}\right) \tag{2}$$

Now consider an elastic crack-tip field dominated by plane strain Mode-I crack. Suppose that a crack is along the horizontal orientation and the tensile crack loading is in the vertical direction. Hence the ratio of in-plane shear mode and opening mode stress intensity factors $K_{II}/K_I << 1$ [20]. Assume that near the crack tip there is a flexoelectric strain-gradient sensor (m3m flexoelectric material) at (r,θ), which has an angle deviation of α to the radial direction. Polarization is then generated in this SGS due to the strain gradient in the x_1',or x_2' direction (shown in Fig. 1). In this case of plane strain the flexoelectric polarizations (P_1', P_2') in SGS becomes.

$$\begin{aligned} P_1' &= \mu_{11}\frac{\partial \varepsilon_{11}'}{\partial x_1'} + \mu_{12}\frac{\partial \varepsilon_{22}'}{\partial x_1'} + \mu_{44}\frac{\partial \varepsilon_{12}'}{\partial x_2'} \\ P_2' &= \mu_{11}\frac{\partial \varepsilon_{22}'}{\partial x_2'} + \mu_{12}\frac{\partial \varepsilon_{11}'}{\partial x_2'} + \mu_{44}\frac{\partial \varepsilon_{12}'}{\partial x_1'} \end{aligned} \tag{3}$$

where the index prime indicates the coordinate system (x_1',x_2'). $P_1'$and P_2' indicate the charge density on two pairs of sidewalls perpendicular with x_1' and x_2' direction, respectively.

Mode-I Asymptotic Crack-Tip

The flexoelectric polarization can be expressed as function of r, θ, α, K_I and other crack-tip parameters. The first three terms of the asymptotic stress field of the crack may be written as.

$$\begin{bmatrix}\sigma_r \\ \sigma_\theta \\ \sigma_{r\theta}\end{bmatrix} = \frac{K_I}{\sqrt{2\pi r}}\frac{1}{4}\begin{bmatrix}\tilde{\sigma}_r^I \\ \tilde{\sigma}_\theta^I \\ \tilde{\sigma}_{r\theta}^I\end{bmatrix} + T\begin{bmatrix}\tilde{\sigma}_r^t \\ \tilde{\sigma}_\theta^t \\ \tilde{\sigma}_{r\theta}^t\end{bmatrix} + A_{1/2}r^{1/2}\begin{bmatrix}\tilde{\sigma}_r^{3d} \\ \tilde{\sigma}_\theta^{3d} \\ \tilde{\sigma}_{r\theta}^{3d}\end{bmatrix} \tag{4}$$

here the first three terms are due to Mode-I crack loading denoting the contributions of singular opening mode stress, constant stress or T-stress and higher order opening mode stress. These three terms are denoted by the superscript I, t, and $3d$, respectively, and.

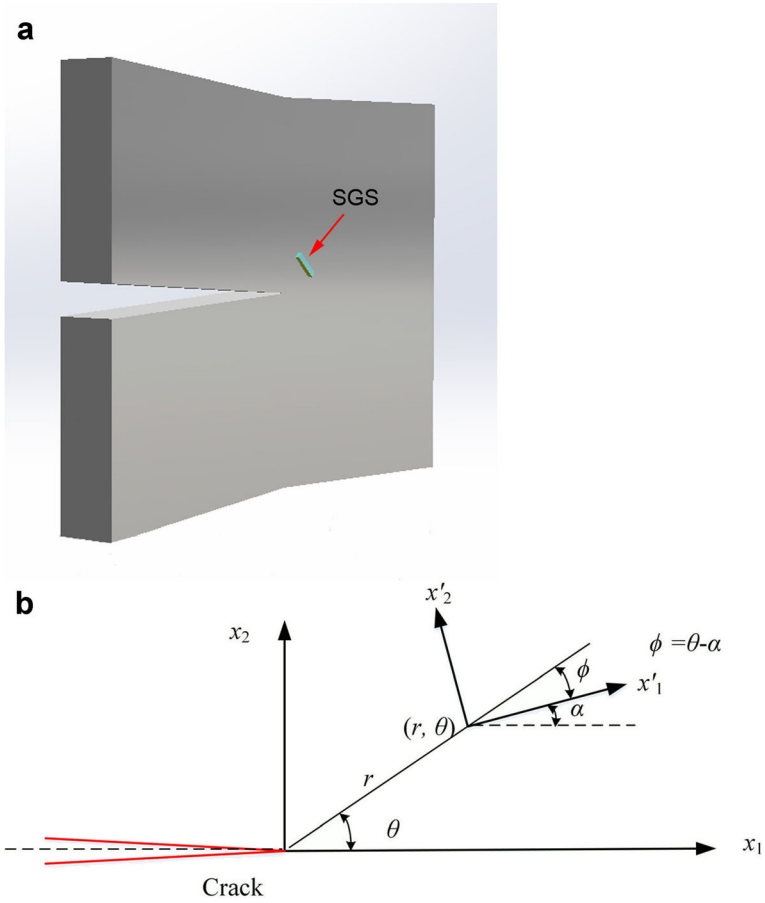

Fig. 1 A mixed-mode crack inclined to a remote tensile field where a strain-gradient sensor is located at (r,θ) to measure strain gradient in the $x_1^{'}$, or $x_2^{'}$ direction

$$\begin{bmatrix} \widetilde{\sigma}_r^I \\ \widetilde{\sigma}_\theta^I \\ \widetilde{\sigma}_{r\theta}^I \end{bmatrix} = \begin{bmatrix} 5\cos\frac{\theta}{2} - \cos\frac{3\theta}{2} \\ 3\cos\frac{\theta}{2} + \cos\frac{3\theta}{2} \\ \sin\frac{\theta}{2} + \sin\frac{3\theta}{2} \end{bmatrix}, \begin{bmatrix} \widetilde{\sigma}_r^t \\ \widetilde{\sigma}_\theta^t \\ \widetilde{\sigma}_{r\theta}^t \end{bmatrix}$$

$$= \begin{bmatrix} \cos^2\theta \\ \sin^2\theta \\ -\sin\theta\cos\theta \end{bmatrix}, \begin{bmatrix} \widetilde{\sigma}_r^{3d} \\ \widetilde{\sigma}_\theta^{3d} \\ \widetilde{\sigma}_{r\theta}^{3d} \end{bmatrix}$$

$$= \begin{bmatrix} 3\cos\frac{\theta}{2} + \cos\frac{5\theta}{2} \\ 5\cos\frac{\theta}{2} - \cos\frac{5\theta}{2} \\ \sin\frac{\theta}{2} - \sin\frac{5\theta}{2} \end{bmatrix} \tag{5}$$

Based on the coordinate transformation law, the stresses in $x_1^{'}$ - $x_2^{'}$ coordinate can be expressed as

$$\begin{aligned} \sigma_{11}^{'} &= \sigma_r \cos^2\phi + \sigma_\theta \sin^2\phi - \sigma_{r\theta} \sin 2\phi \\ \sigma_{22}^{'} &= \sigma_r \sin^2\phi + \sigma_\theta \cos^2\phi + \sigma_{r\theta} \sin 2\phi \\ \sigma_{12}^{'} &= \frac{\sigma_r - \sigma_\theta}{2} \sin 2\phi + \sigma_{r\theta} \cos 2\phi \end{aligned} \tag{6}$$

where $\phi=\theta-\alpha$, and Hooke's law gives the strain expressions

$$\begin{aligned} \varepsilon_{11}^{'} &= \frac{1-\nu^2}{E}\left(\sigma_{11}^{'} - \frac{\nu}{1-\nu}\sigma_{22}^{'}\right) \\ \varepsilon_{22}^{'} &= \frac{1-\nu^2}{E}\left(\sigma_{22}^{'} - \frac{\nu}{1-\nu}\sigma_{11}^{'}\right) \\ \varepsilon_{12}^{'} &= \frac{1}{2G}\sigma_{12}^{'} \end{aligned} \tag{7}$$

where E is the Young's modulus, G the shear modulus and ν the Poisson's ratio. Substituting stresses in (6) into (7), the expressions for the strain can be obtained as

$$\begin{aligned} E'\varepsilon_{11}^{'} &= \frac{K_I}{\sqrt{2\pi r}}\frac{1}{4}\widetilde{\varepsilon}_1^I + T\widetilde{\varepsilon}_1^t + A_{1/2}\sqrt{r}\widetilde{\varepsilon}_1^{3d} \\ E'\varepsilon_{22}^{'} &= \frac{K_I}{\sqrt{2\pi r}}\frac{1}{4}\widetilde{\varepsilon}_2^I + T\widetilde{\varepsilon}_2^t + A_{1/2}\sqrt{r}\widetilde{\varepsilon}_2^{3d} \\ 2G\varepsilon_{12}^{'} &= \frac{K_I}{\sqrt{2\pi r}}\frac{1}{4}\widetilde{\varepsilon}_{12}^I + T\widetilde{\varepsilon}_{12}^t + A_{1/2}\sqrt{r}\widetilde{\varepsilon}_{12}^{3d} \end{aligned} \tag{8}$$

where

$$\widetilde{\varepsilon}_1^n = \widetilde{\sigma}_r^n c_{ms} + \widetilde{\sigma}_\theta^n s_{mc} - (1+\nu')\widetilde{\sigma}_{r\theta}^n \sin 2\phi$$

$$\widetilde{\varepsilon}_2^n = \widetilde{\sigma}_r^n s_{mc} + \widetilde{\sigma}_\theta^n c_{ms} + (1+\nu')\widetilde{\sigma}_{r\theta}^n \sin 2\phi \quad n = I,\ t,\ 3d$$

$$\widetilde{\varepsilon}_{12}^n = \frac{\widetilde{\sigma}_r^n - \widetilde{\sigma}_\theta^n}{2}(1+\nu')\sin 2\phi + \widetilde{\sigma}_{r\theta}^n (1+\nu')\cos 2\phi \tag{9}$$

and

$$\begin{aligned} c_{ms} &= \cos^2\phi - \nu' \sin^2\phi = [1 - \nu' + (1+\nu')\cos 2\phi]/2 \\ s_{mc} &= \sin^2\phi - \nu' \cos^2\phi = [1 - \nu' - (1+\nu')\cos 2\phi]/2 \\ E' &= \frac{E}{1-\nu^2},\ \ \nu' = \frac{\nu}{1-\nu} \end{aligned} \tag{10}$$

As the above expressions for the strains are functions of (r,θ), differential relations can be established.

$$\begin{aligned} &\frac{\partial \varepsilon'_{11}}{\partial \varepsilon'_1} = \cos\phi \frac{\partial \varepsilon'_1}{\partial r} - \frac{\sin\phi}{r}\frac{\partial \varepsilon'_{11}}{\partial \theta}, \quad \frac{\partial \varepsilon'_{22}}{\partial \varepsilon'_1} = \cos\phi \frac{\partial \varepsilon'_{22}}{\partial r} - \frac{\sin\phi}{r}\frac{\partial \varepsilon'_{22}}{\partial \theta} \\ &\frac{\partial \varepsilon'_{12}}{\partial \varepsilon'_2} = \sin\phi \frac{\partial \varepsilon'_{12}}{\partial r} + \frac{\cos\phi}{r}\frac{\partial \varepsilon'_{12}}{\partial \theta}, \quad \frac{\partial \varepsilon'_{22}}{\partial \varepsilon'_2} = \cdots \\ &\cdots\cdots \end{aligned} \tag{11}$$

Asymptotic strain gradient expansions near the crack tip can thus be expressed as

$$\begin{aligned} E'\frac{\partial \varepsilon'_{11}}{\partial \varepsilon'_1} &= -\frac{K_I}{r\sqrt{2\pi r}}\frac{1}{8}\left(\widetilde{\varepsilon}_1^I \cos\phi + 2\widetilde{\varepsilon}_{1,\theta}^I \sin\phi\right) - T\widetilde{\varepsilon}_{1,\theta}^t \frac{\sin\phi}{r} + \frac{A_{1/2}}{2\sqrt{r}}\left(\widetilde{\varepsilon}_1^{3d}\cos\phi - 2\widetilde{\varepsilon}_{1,\theta}^{3d}\sin\phi\right) \\ E'\frac{\partial \varepsilon'_{22}}{\partial \varepsilon'_1} &= -\frac{K_I}{r\sqrt{2\pi r}}\frac{1}{8}\left(\widetilde{\varepsilon}_2^I \cos\phi + 2\widetilde{\varepsilon}_{2,\theta}^I \sin\phi\right) - T\widetilde{\varepsilon}_{2,\theta}^t \frac{\sin\phi}{r} + \frac{A_{1/2}}{2\sqrt{r}}\left(\widetilde{\varepsilon}_2^{3d}\cos\phi - 2\widetilde{\varepsilon}_{2,\theta}^{3d}\sin\phi\right) \\ 2G\frac{\partial \varepsilon'_{12}}{\partial \varepsilon'_2} &= -\frac{K_I}{r\sqrt{2\pi r}}\frac{1}{8}\left(\widetilde{\varepsilon}_{12}^I \sin\phi - 2\widetilde{\varepsilon}_{12,\theta}^I \cos\phi\right) + T\widetilde{\varepsilon}_{12,\theta}^t \frac{\cos\phi}{r} + \frac{A_{1/2}}{2\sqrt{r}}\left(\widetilde{\varepsilon}_{12}^{3d}\sin\phi + 2\widetilde{\varepsilon}_{12,\theta}^{3d}\cos\phi\right) \\ \frac{\partial \varepsilon'_{22}}{\partial \varepsilon'_2} &= \cdots, \qquad \cdots\cdots \end{aligned} \tag{12}$$

where $\widetilde{\varepsilon}_{ij}^n \ \ (n = I,\ t,\ 3d)$ are given by equation. (9), the derivatives $\widetilde{\varepsilon}_{ij,\theta}^n$ can be derived to be

$$\begin{aligned} \widetilde{\varepsilon}_{1,\theta}^n &= \widetilde{\sigma}_{r,\theta}^n c_{ms} + \widetilde{\sigma}_r^n c'_{ms} + \widetilde{\sigma}_{\theta,\theta}^n s_{mc} + \widetilde{\sigma}_\theta^n s'_{ms} - (1+\nu') \\ &\quad \left(\widetilde{\sigma}_{r\theta,\theta}^n \sin 2\phi + 2\widetilde{\sigma}_{r\theta}^n \cos 2\phi\right) \\ \widetilde{\varepsilon}_{2,\theta}^n &= \widetilde{\sigma}_{r,\theta}^n s_{mc} + \widetilde{\sigma}_r^n s'_{ms} + \widetilde{\sigma}_{\theta,\theta}^n c_{ms} + \widetilde{\sigma}_\theta^n c'_{ms} + (1+\nu') \\ &\quad \left(\widetilde{\sigma}_{r\theta,\theta}^n \sin 2\phi + 2\widetilde{\sigma}_{r\theta}^n \cos 2\phi\right) \\ \widetilde{\varepsilon}_{12,\theta}^n &= \frac{\widetilde{\sigma}_{r,\theta}^n + \widetilde{\sigma}_{\theta,\theta}^n - 4\widetilde{\sigma}_{r\theta}^n}{2}\sin 2\phi + \left(\widetilde{\sigma}_r^n + \widetilde{\sigma}_\theta^n + \widetilde{\sigma}_{r\theta,\theta}^n\right)\cos 2\phi \end{aligned} \tag{13}$$

$$c'_{ms} = -(1+\nu')\sin 2\phi \qquad s'_{ms} = (1+\nu')\sin 2\phi \tag{14}$$

Therefore, the polarizations P'_1, P'_2 in the $x'_1$and x'_2 directions near the mixed mode crack tip are obtained as

$$\begin{aligned} P'_1 &= \frac{1}{E'}\left(-\frac{K_I}{8\sqrt{2\pi}r^{3/2}}P_1^I(\theta,\phi) + \frac{T}{r}P_1^T(\theta,\phi) + \frac{A_{1/2}}{2\sqrt{r}}P_1^{3d}(\theta,\phi)\right) \\ P'_2 &= \frac{1}{E'}\left(-\frac{K_I}{8\sqrt{2\pi}r^{3/2}}P_2^I(\theta,\phi) + \frac{T}{r}P_2^T(\theta,\phi) + \frac{A_{1/2}}{2\sqrt{r}}P_2^{3d}(\theta,\phi)\right) \end{aligned} \tag{15}$$

where

$$\begin{aligned} P_1^I(\theta,\phi) &= \mu_{11}\left(\widetilde{\varepsilon}_1^I\cos\phi + 2\widetilde{\varepsilon}_{1,\theta}^I\sin\phi\right) + \mu_{12}\left(\widetilde{\varepsilon}_2^I\cos\phi + 2\widetilde{\varepsilon}_{2,\theta}^I\sin\phi\right) \\ &\quad + \mu_{44}(1+\nu')\left(\widetilde{\varepsilon}_{12}^I\sin\phi - 2\widetilde{\varepsilon}_{12,\theta}^I\cos\phi\right) \\ P_1^T(\theta,\phi) &= -\left(\mu_{11}\widetilde{\varepsilon}_{1,\theta}^t + \mu_{12}\widetilde{\varepsilon}_{2,\theta}^t\right)\sin\phi + \mu_{44}(1+\nu')\widetilde{\varepsilon}_{12,\theta}^t\cos\phi \\ P_1^{3d}(\theta,\phi) &= \mu_{11}\left(\widetilde{\varepsilon}_1^{3d}\cos\phi - 2\widetilde{\varepsilon}_{1,\theta}^{3d}\sin\phi\right) + \mu_{12}\left(\widetilde{\varepsilon}_2^{3d}\cos\phi - 2\widetilde{\varepsilon}_{2,\theta}^{3d}\sin\phi\right) \\ &\quad + \mu_{44}(1+\nu')\left(\widetilde{\varepsilon}_{12}^{3d}\sin\phi + 2\widetilde{\varepsilon}_{12,\theta}^{3d}\cos\phi\right) \\ P_2^I(\theta,\phi) &= \cdots\cdots \end{aligned} \tag{16}$$

The expressions for the polarization includes the following parameters: three flexoelectric coefficients of the SGS sensor

(μ_{11}, μ_{12}, μ_{44}), three loading parameters of the crack-tip field (K_I, T, $A_{1/2}$), and three geometric parameters (r,θ, α).

Evaluation of K_I by Asymptotic Polarization Expansions

The asymptotic crack-tip expansions of the SGS polarization provide theoretical estimation of the SGS polarization near the crack tip. Reversely, crack intensity factor can be evaluated given the flexoelectric coefficients (μ_{11}, μ_{12}, μ_{44}) and the relative orientation parameters (r,θ, α) of SGS near a crack tip, stress intensity factor and other crack-tip parameters (K_I, T, $A_{1/2}$) can be evaluated using experimentally measured electric polarization of SGS. First two terms in the stress expression are considered here by ignoring the high order terms, which is commonly an accurate simplification of practical application.

Shear flexoelectricity is supposed to be trivial compared with axial and transverse components [15], which are in similar order and commonly assumed equal [21]. By substituting equations. (5), (9), (13) into equation. (16), $P_1^T(\theta,\phi)$ can be found to be zero, and the flexoelectric polarization can be simplifed as

$$P_1^{'} = \frac{1}{E'}\left(-\frac{K_I}{\sqrt{2\pi}r^{3/2}}8\cos\frac{\theta}{2}\mu(1-\nu')\right) = \frac{(1+\nu)(1-2\nu)\mu}{E}\left(-\frac{K_I}{\sqrt{2\pi}r^{3/2}}\cos\left(\frac{\theta}{2}+\phi\right)\right) \quad (17)$$

where μ is the flexoelectric coefficient of the SGS material. Thus the effect of constant stress could be eliminated, which otherwise couples with K_I component and suppress the accurate determination of Mode-I stress intensity factor. [20] Dismiss of constant stress component in the flexoelectric output is expected taking into account of nature of strain gradient. In contrast, the effect of constant stress always exists in strain measurement using strain gauges. The constant stress term could contribute more than 20 % for the total stress distribution in the field with the polar radius of $0.1a$, where a is the crack length [20]. To remove the impact, strain gauge should be placed along a particular orientation which is a function of Poisson's ratio [7]. This leads to a narrow sensor mounting area for obtaining accurate measurement. Thus stress intensify factor measurement results can be susceptible to the localization error of strain gauges. For flexoelectric SGS measurements, there is no similar limitation, due to the independence of SGS output upon the constant stress. SGS sensor can be placed across a large area, which potentially improves the accuracy of stress intensify factor measurement.

Experimental Measurement of K_I

BST SGS Fabrication

$Ba_xSr_{1-x}TiO_3$ (BST) ceramic presented the highest flexoelectric coefficients among all reported ferroelectric materials up to now [14]. In this study, BST with the composition of Ba:Sr=64 %:36 % was lab-prepared using a conventional solid state processing method. The Young's modulus of the BST is 152 GPa and Poisson ratio is 0.33 [22]. The Curie temperature of the prepared BST samples was measured to be 18 ˚C and the dielectric constant at room temperature was measured as 14,000. Impedance analysis of the ceramic showed no resonant or anti-resonant frequency in the frequency range of 40 Hz to 110 MHz at room temperature, indicating that the prepared BST samples are not piezoelectrics. By using the cantilever beam based direct measurement introduced in another paper [16], the transverse flexoelectric coefficient μ_{12} was measured to be about 45μC/m. BST micro-bars (4.7 mm×0.9 mm×0.3 mm) were obtained by lapping and polishing. The induced charge should be collected at the electrodes on the sidewalls (4.7 mm×0.9 mm) of the sensors. Coaxial wires were bonded to the sidewall electrodes using silver paste to eliminate the external noise. Epoxy adhesive (Hysol EA 9359.3) was used to bond the SGS to the aluminum substrate.

Selection of SGS Coordinates

From the equation. (17), the flexoelectric output of the SGS is a simple function of angular position θ and orientation ϕ. Based on this equation, the SGS would yield the maximum output when attached at along the horizontal direction. It is well known that strain gauge should not be placed very close (within a distance of the plate thickness) to the crack tip to avoid three dimensional effect and other factors which make the two dimensional plane stress solution invalid. On the other hand the strain gauge cannot be placed too far from the crack tip because the singular solution may not be dominant in that region. These constrains also applied to SGS placement due to the same stress distribution near the crack tip.

Effect of SGS Size

The measured flexoelectric output is actually an average effect across the whole area of the SGS. As the SGS has a finite area, the strain gradient varies at different spots. The expected output at the centroid of the SGS is used here for back calculation of K_I. This could induce a certain magnitude of error, especially when the SGS is amounted close to the crack tip. This error can be estimated as following. Consider a SGS attached along the horizontal direction with a distance of r_c to the crack tip. The width of the SGS is w while the length is L,

as shown in Fig. 2. The polar angle sweeps across $2\theta_0$ with θ_0=atan($L/2r_c$), r_1=r_c -w/2 and r_2=r_c+w/2.

The average flexoelectric polarization can be attained through integration over the whole area, due to the small size of the SGS, it can be approximated to an arc shape geometry for estimation. The averaged flexoelectric output can be written as

$$P_{ave} = K\frac{\int_{-\theta_0}^{\theta_0}\int_{r_1}^{r_2}\frac{1}{r^{3/2}}\cos\frac{\theta}{2}drd\theta}{wL} \tag{18}$$

where K is a constant value related to K_I. The output at the center point has the expression of.

$$P_c = K\frac{1}{r_c^{3/2}} \tag{19}$$

The ratio between the averaged output with the center value is plotted in Fig. 3 as a function of normalized SGS position (1 means that the ratio of r_c to L equals to 1). The width of the SGS is assumed to be one fifth of the length, which is a good approximation of the real sensor dimension. The averaged value is found to be 10 % less than the center value when the SGS is placed adjacent to the crack tip. As the distance enlarges, the difference decreases rapidly.

Crack Loading Test

A specimen with width b=76.2 mm and length of 300 mm were fabricated from a 3.2 mm thick plate of aluminum 2024-T851. An edge crack was generated by applying fatigue loading onto a crack starter notch with the length of 34 mm prototyped on the specimen. In order to demonstrate the capability of SGS in measuring stress intensity factor, uniaxial load was applied and only the opening mode crack was considered. The critical stress intensity factor K_{IC} of aluminum is given as 23 MPa·m$^{-1/2}$, Poisson ratio is 0.3 and young's modulus is 70 GPa. For the maximum endurable load, the plastic zone is estimated to be less than 2.7 mm in radius. [20] K_I at the crack tip under a uniaxial stress σ can be empirically evaluated as [23]

$$K_I = \sigma\sqrt{\pi a}\left[1.12-0.23\left(\frac{a}{b}\right)+10.6\left(\frac{a}{b}\right)^2-21.7\left(\frac{a}{b}\right)^3+30.4\left(\frac{a}{b}\right)^4\right] \tag{20}$$

where a is the crack length, and the expression is valid outside the plastic zone around the crack tip.

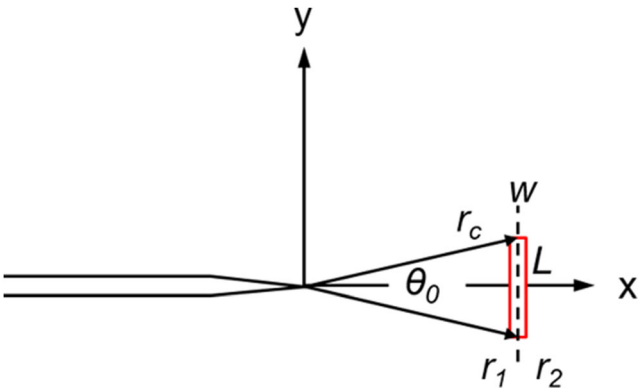

Fig. 2 Definition of dimension parameters with SGS placement near the crack tip

The crack initiated along the starter notch and propagated with a final length of 3.7 mm. To simplify the case and make a direct comparison with theoretical estimation of K_I, two SGSs were attached to the specimen along the horizontal direction. The distances to the crack tip were chosen to be about one and two times of the sensor length, respectively. In order to compare the strain gradient based measurement method with traditional strain associated approach, a commercial strain gauge (Micro-Measurement EA-06-125BB-12 was attached near the crack to attain K_I value. The strain gauge was located at a special angle of 60° along the horizontal orientation to cancel the strain contribution from the uncertain constant stress component. [7] The calculation of this angle necessitates the acquirement of Poisson's ratio of materials. The placement of SGS and strain gauge was shown in Fig. 4. The locations of SGSs and strain gauge on the specimen are given in Table 1. Experiment was conducted on a hydraulic tester (Instron 1331). The charge output from the SGS was monitored using a charge amplifier (Bruel & Kjaer 2635), with the stress swept from 2 MPa to 7 MPa at 1 Hz. The

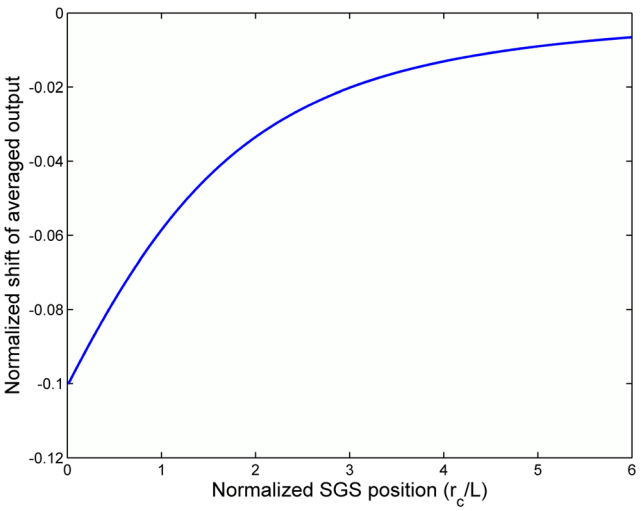

Fig. 3 Normalized shift of averaged flexoelectric output as a function of normalized SGS position r_c/L

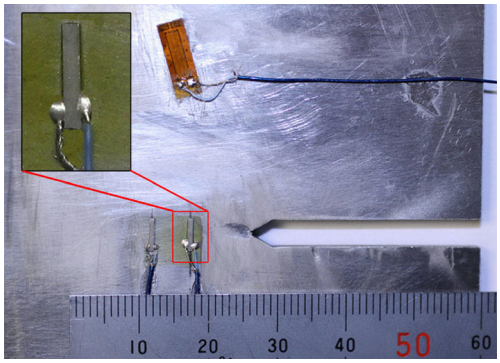

Fig. 4 Photography of crack with two SGSs attached at different locations

charge to voltage conversion coefficient was set to be 10 mV/pC and the output was read by a digital oscilloscope (DSO7104B, Agilent Technologies Inc.). The relative low stress level was chosen to prevent the crack growth by fatigue loading, as the experiment lasted for a long period of time which involved numerous cycles.

Assume μ_{11} has the same value of μ_{12} (measured value of 45 μC/m) and neglect μ_{44} [24], K_I can be calculated from measured charge signal of SGSs based on equation. (17). The voltage output read from the oscilloscope is in 100 mV level under high stress. Comparison between empirical calculation and measured results from SGSs and strain gauge were presented in Fig. 5. It can be observed that measured values from SGS-2 and strain gauge match well with theoretical estimations. Only the first data point is off the theoretical trend, this may be caused by a non-negligible measurement error under low loading level, i.e. the stress applied by the tester is not sufficiently accurate or the charge output reading is low. Small deviations exist between the experimental results from SGS-1 and the theoretical data with a magnitude about 10 %. Based on the previous error analysis, the real flexoelectric output is smaller than the center spot value by 10 % as the SGS is attached close to the crack tip. Since the center point dimension parameter was used to back estimate the stress intensity factor, the real factor value should be larger than the estimated one, as observed in the experiment. This error diminishes as

Table 1 Geometry dimensions of SGSs and strain gauge. K_I results and the difference between theoretical and experimental results for 1500 lb load

	SGS-1	SGS-2	Strain gauge
Distance from crack tip	5.4 mm	10.4 mm	25 mm
θ	0 °	0 °	60 °
ϕ	0 °	0 °	0 °
Measured K_I (MPa $m^{1/2}$)	5.16	5.42	5.92
Empirical K_I (MPa $m^{1/2}$)	5.73	5.73	5.73
Difference percent	−10	−5	3

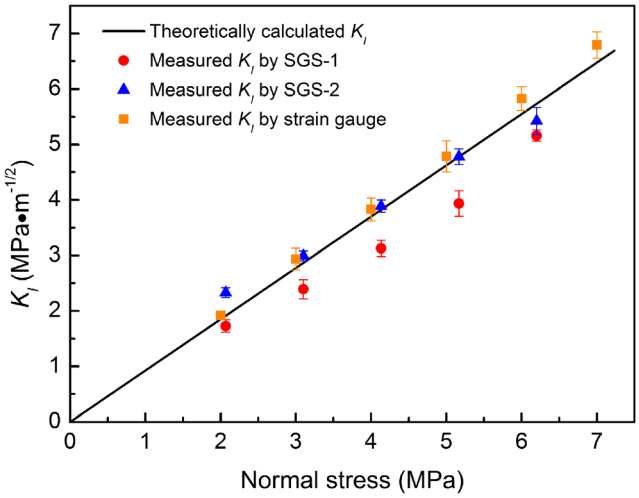

Fig. 5 Comparison of empirical estimation of Mode-I stress intensity factor K_I and measured results from two SGSs and one strain gauge

the polar radius increases, explaining the decreased discrepancy between the SGS-2 results with the theoretical expectation. Several other sources could contribute to the experimental results errors. A certain measurement error lies in the locating of the crack tip which represents the origin of the (r,θ) coordinate system. Difficulties in identifying the location of the crack tip also produce errors in measuring the relative positions of SGSs. In addition, the fatigue-initiated crack tip shows a curved crack front and has an angle with the mechanically prototyped regular crack starter notch. This compromises the accuracy of empirical model which assumes a straight crack trace line. In spite of this, strain gradient sensor attached away from the close area of cracks could easily provide an appropriate estimation of the open mode stress intensity factor. We believe that with the consideration of all these factors, SGS offers a convenient approach for stress intensity factor measurement.

Summary

The measurement of opening mode stress intensify factor of crack was analyzed by using strain gradient sensors. The effect of constant stress component in precisely determining the stress intensity factor K_I can be eliminated by SGS assisted measurement, attributed to the nature of strain gradient. This unique property removes the special requirement for sensor coordinates required in strain gauge measurements. Experiments conducted to verify the theory show that the measured opening mode K_I values using strain gradient sensor match well with the empirical estimation and experimental results from strain gauge measurement. The size effect of the SGS was studied as a function of radical distance to the crack tip. The small measurement errors from the strain gradient

sensor in the near field are due mainly to the finite size of SGS. Overall, SGS provides a convenient and new method for characterizing the opening mode stress intensity factor.

Acknowledgments This material is based on work supported by, or in part by, the US Army Research Laboratory and the US Army Research Office under contract/grant number W911NF-11-1-0516 and in part by National Science Foundation under grant number CMMI-1068345. We also appreciate De Zhang and Jared Little's help for the experimental implementation.

References

1. Boller C (2000) Next generation structural health monitoring and its integration into aircraft design. Int J Syst Sci 31(11):1333–1349
2. Rybicki EF, Kanninen MF (1977) A finite element calculation of stress intensity factors by a modified crack closure integral. Eng Fract Mech 9(4):931–938
3. Etheridge J, Dally J (1977) A critical review of methods for determining stress-intensity factors from isochromatic fringes. Exp Mech 17(7):248–254
4. Hild F, Roux S (2006) Measuring stress intensity factors with a camera: Integrated digital image correlation (I-DIC). Comptes Rendus Mécanique 334(1):8–12
5. Clark AV, Mignogna RB, Sanford RJ (1983) Acousto-elastic measurement of stress and stress intensity factors around crack tips. Ultrasonics 21(2):57–64
6. Díaz FA, Patterson EA, Tomlinson RA, Yates JR (2004) Measuring stress intensity factors during fatigue crack growth using thermoelasticity. Fatigue Fract Eng Mater Struct 27(7):571–583
7. Dally JW, Sanford RJ (1987) Strain-gage methods for measuring the opening-mode stress-intensity factor. Exp Mech 27(4):381–388
8. Fujimoto Y, Shintaku E, Pirker G, Liu G (2003) Piezoelectric sensor for stress intensity factor measurement of two dimensional cracks. Eng Fract Mech 70(9):1203–1218
9. Huang W, Yan X, Kwon SR, Zhang S, Yuan FG, Jiang X (2012) Flexoelectric strain gradient detection using $Ba_{0.64}Sr_{0.36}TiO_3$ for sensing. Appl Phys Lett 101(25):252903
10. Kogan SM (1964) Piezoelectric effect during inhomogeneous deformation and acoustic scattering of carriers in crystals. Sov Phys Solid State 5(10):2069–2070
11. Tagantsev AK (1986) Piezoelectricity and flexoelectricity in crystalline dielectrics. Phys Rev B 34(8):5883–5889
12. Tagantsev AK (1991) Electric polarization in crystals and its response to thermal and elastic perturbations. Phase Transit 35(3–4):119–203
13. Cross LE (2006) Flexoelectric effects: charge separation in insulating solids subjected to elastic strain gradients. J Mater Sci 41(1):53–63
14. Ma WH, Cross LE (2002) Flexoelectric polarization of barium strontium titanate in the paraelectric state. Appl Phys Lett 81(18):3440–3442
15. Maranganti R, Sharma P (2009) Atomistic determination of flexoelectric properties of crystalline dielectrics. Phys Rev B 80(5): 054109
16. Huang WB, Kim K, Zhang SJ, Yuan FG, Jiang XN (2011) Scaling effect of flexoelectric (Ba, Sr)TiO3 microcantilevers. Phys Status Solidi-Rapid Res Lett 5(9):350–352
17. Huang W, Kwon SR, Zhang S, Yuan FG, Jiang X (2013) A trapezoidal flexoelectric accelerometer. J Intel Mat Syst Str. doi:10.1177/1045389X13491021
18. Shen Z, Chen W (2012) Converse flexoelectric effect in comb electrode piezoelectric microbeam. Phys Lett A 376(19):1661–1663
19. Qi Y, Kim J, Nguyen TD, Lisko B, Purohit PK, McAlpine MC (2011) Enhanced piezoelectricity and stretchability in energy harvesting devices fabricated from buckled PZT ribbons. Nano Lett 11(3): 1331–1336
20. Anderson TL (2005) Fracture mechanics: fundamentals and applications. CRC press, Boca Raton
21. Ma WH (2010) Flexoelectric charge separation and size dependent piezoelectricity in dielectric solids. Phys Status Solidi B 247(1):213–218
22. Zhu WY, Fu JY, Li N, Cross L (2006) Piezoelectric composite based on the enhanced flexoelectric effects. Appl Phys Lett 89(19):192904
23. Gross D, Seelig T (2011) Fracture mechanics: with an introduction to micromechanics. Springer, Verlag Berlin Heidelberg
24. Shu L, Wei X, Pang T, Yao X, Wang C (2011) Symmetry of flexoelectric coefficients in crystalline medium. J Appl Phys 110(10):104106